MIT Open Access Articles

Infrared absorption of n-type tensile-strained Ge-on-Si

Infrared absorption of *n*-type tensile-strained Ge-on-Si

Xiaoxin Wang,[1] Haofeng Li,[1] Rodolfo Camacho-Aguilera,[2] Yan Cai,[2] Lionel C. Kimerling,[2]
Jurgen Michel,[2] and Jifeng Liu[1,*]

[1]*Thayer School of Engineering, Dartmouth College, Hanover, New Hampshire 03755, USA*

[2]*Department of Materials Science and Engineering, Microphotonics Center, Massachusetts Institute of Technology,
Cambridge, Massachusetts 02139, USA*

Corresponding author: jifeng.liu@dartmouth.edu

We analyze the IR absorption of tensile-strained, *n*-type Ge for Si-compatible laser applications. A strong intervalley scattering from the indirect L valleys to the direct Γ valley in n^+ Ge-on-Si is reported for the first time to our knowledge. The intervalley absorption edge is in good agreement with the theoretical value. On the other hand, we found that the classical λ^2-dependent Drude model of intravalley free-carrier absorption (FCA) breaks down at $\lambda < 15$ μm. A first-principle model has to be employed to reach a good agreement with the experimental data. The intravalley FCA loss is determined to be <20 cm^{-1} for $n = 4 \times 10^{19}$ cm^{-3} at $\lambda = 1.5$–1.7 μm, an order lower than the results from Drude model. The strong $L \to \Gamma$ intervalley scattering favors electronic occupation of the direct Γ valley, thereby enhancing optical gain from the direct gap transition of Ge, while the low intravalley free-electron absorption at lasing wavelengths leads to low optical losses. These two factors explain why the first electrically pumped Ge-on-Si laser achieved a higher net gain than the theoretical prediction using λ^2-dependent free-carrier losses of bulk Ge and indicate the great potential for further improvement of Ge-on-Si lasers.   © 2013 Optical Society of America

    OCIS codes: 130.3130, 160.3380, 250.5960.

In recent years, epitaxial Ge-on-Si has been applied to integrated active photonic devices based on its direct bandgap transition [1–4]. Especially, lasing from the direct gap transition of tensile-strained n^+ Ge-on-Si has been successfully demonstrated under optical [5] and electrical pumping [6]. In these devices, tensile strain reduces the energy difference between the direct (Γ) and indirect (L) conduction valleys, while *n*-type doping compensates the rest of the energy difference [3]. For the first electrically pumped Ge-on-Si laser, a net gain >500 cm^{-1} is achieved from the direct gap transition of 0.2% tensile-strained Ge with $n = 4 \times 10^{19}$ cm^{-3} [6]. Remarkably, the *n*-type doping level for such a large gain coefficient is only half of the theoretical value calculated using λ^2-dependent free-carrier absorption (FCA) losses of bulk Ge [3]. The discrepancy between theoretical modeling and experimental data needs to be investigated in order to gain more understanding to further optimize Ge-on-Si lasers.

In this Letter, we report a strong $L \to \Gamma$ intervalley scattering at $\lambda < 10$ μm and a weak intra-L-valley FCA loss in the lasing wavelength regime of $\lambda = 1.5$–1.7 μm [6] from the IR absorption spectra of tensile-strained n^+ Ge-on-Si gain media. The $L \to \Gamma$ intervalley absorption edge is in good agreement with theoretical value. On the other hand, the λ^2-dependent Drude model of FCA only holds true at $\lambda \geq 15$ μm. A first-principle model of intravalley transitions has to be employed to reach an agreement with the experimental data of intra-L-valley FCA, which turns out to be negligible in the lasing wavelength range of 1.5–1.7 μm. The strong $L \to \Gamma$ intervalley scattering favors electronic occupation of the direct Γ valley to enhance the direct gap optical gain of n^+ Ge, while the low intravalley free-electron absorption at lasing wavelengths leads to low optical losses. These two factors explain why the first electrically pumped Ge-on-Si laser achieved a higher net gain than the theoretical calculation based on λ^2-dependent infrared absorption data of bulk Ge. These results also indicate that Ge-on-Si laser

can potentially achieve an even better performance than our original theoretical prediction in [3].

Epitaxial Ge films with phosphorus (P) doping were grown on Si by ultrahigh-vacuum chemical vapor deposition [4,6]. The thermally induced tensile strain in the Ge layer is 0.2%–0.25% [7]. The *P*-doping profiles were measured by secondary ion mass spectrometry. The free-electron concentrations were determined by Hall effect measurements, ranging from 7×10^{18} to 4×10^{19} cm^{-3}.

To investigate the infrared absorption of n^+ Ge films, the transmittance spectra were measured with a JASCO FTIR-4100 spectrometer in the wavelength range of 1.3–22 μm. Figures 1(a) and 1(b) show the transmittance spectra of samples D1–D3 together with their single side polished (SSP) Si substrates as references. The Ge film thicknesses and doping concentrations in these samples are D1 (740 nm, 1×10^{19} cm^{-3}), D2 (651 nm, 2.9×10^{19} cm^{-3}), and D3 (651 nm, 3.9×10^{19} cm^{-3}). D2 and D3 also have 100 nm thick SiO$_2$ cap layers. The broad oscillations in the wavelength range of 1–5 μm are produced by the multilayer interference effect. Because of the wavelength-dependent scattering caused by the backside roughness of SSP Si and impurity IR absorption in Si [8,9], the transmittance of SSP Si substrates deviates from the theoretical value of ∼55% in the wavelength range of 1.3–22 μm. In particular, the dips in the transmission spectra at ∼9 and ∼16.5 μm correspond to the absorption due to oxygen and carbon in the Si substrate, respectively [10,11]. In order to single out the absorption coefficients of n^+ Ge thin films from the transmittance spectra, we first derive effective absorption coefficients of the SSP Si substrate from its transmittance data, which takes into account the backside roughness scattering and impurity infrared absorption. The refractive index of the SiO$_2$ layer is obtained by ellipsometry. Then with a combination of transfer matrix analysis and the Kramers–Kronig relation we were able to derive the absorption coefficient as well as the real part of refractive index for the tensile-strained n^+ Ge thin films deterministically
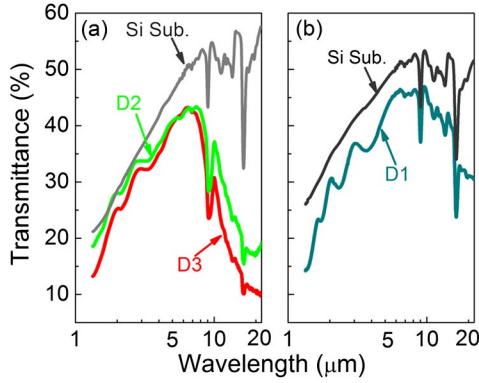
Fig. 1.   (Color online) (a), (b) Transmittance spectra of 0.25% tensile-strained n^+ Ge-on-Si samples D1–D3 together with their SSP Si substrates as references.

using an iterative self-consistent regression approach [7]. The validity of this method has been verified by deriving the optical constants of SiO_2 in the mid- and far-IR regime from the raw transmission data of SiO_2 thin films on SSP Si substrates reported in [9]. The derived absorption coefficient and real part of refractive index using our method are in good agreement with the results in [9].

As an example, Fig. 2 shows the IR absorption spectrum of Ge thin film with $n = 1 \times 10^{19}$ cm^{-3} derived from the transmittance data of D1. The absorption spectrum can be divided into four regimes. In Regime I the absorption drastically increases with wavelength at $\lambda > 10$ μm, indicating FCA. For n-type bulk Ge with $n = 1 \times 10^{18} \sim 5 \times 10^{19}$ cm^{-3}, the characteristic λ^2-dependent FCA based on the Drude model is commonly observed in the wavelength range of 2–40 μm [12–15]. As a comparison, the λ^2-dependent Drude model is shown with the dashed green line. While the observed FCA largely follows λ^2-dependence at $\lambda > 15$ μm, it decreases much faster with wavelength than the λ^2 model at $\lambda < 11$ μm. This deviation from the Drude model is in good agreement with our first-principle calculation of Ge FCA (dashed magenta line in Fig. 2) following the approach in [16], which takes into account the band structure as well as optical phonon, acoustic phonon, and charged impurity scattering mechanisms. The parameters of Ge used in the model are effective mass of L-valley electron $m_e^L = 0.22m_0$,
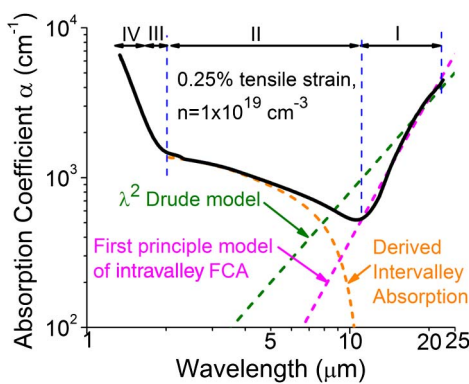

Fig. 2.   (Color online) IR absorption spectrum of Ge thin film with $n = 1 \times 10^{19}$ cm^{-3} derived from the transmittance data of D1. Regimes I–IV are dominated by intra-L-valley FCA, $L \to \Gamma$ IVSA, indirect gap + intervalley scattering absorption, and direct gap absorption, respectively.

optical phonon energy $\hbar\omega_{opt} = 37$ meV, average velocity of sound $v_s = 4.18$ m/s, deformation potential of optical phonons $D_O = 5.5 \times 10^{10}$ eV/m, and deformation potential of acoustic phonons $D_A = 8.84$ eV [17]. The first-principle model also indicates that, similar to GaAs [16], the scattering by donor ions is the dominant FCA mechanism in n^+ Ge at $\lambda = 10$–22 μm since it is the most efficient one in transferring small momenta to electrons, as required for FCA at long wavelengths. On the other hand, the intravalley FCA of higher-energy near-IR photons requires a large momentum transfer so that the deformation potential acoustic phonon mechanism dominates the transition [16]. Considering Bose distribution, the small population of high momentum (thus high energy) acoustic phonons leads to a low intravalley FCA at shorter wavelengths [16]. Using the first-principle model, we determined that the intra-L-valley FCA is <20 cm^{-1} in the Ge laser wavelength regime of $\lambda = 1.5$–1.7 μm for $n \leq 3.9 \times 10^{19}$ cm^{-3}, an order lower than the FCA data from the Drude model [18]. This result agrees with both [16] and Haug's quantum mechanical analysis showing that intravalley FCA at photon energies larger than the bandgap is of the order of 1 cm^{-1} for mid 10^{18} cm^{-3} n-type doping [19]. It also explains why a higher net gain is achieved for the electrically pumped Ge-on-Si lasers in [6] compared to theoretical calculation using FCA data from the Drude model in [3].

In Regime II, the absorption starts to increase significantly with the decrease of wavelength at $\lambda < 10$ μm, indicating a change in the dominant absorption mechanism. Since 10 μm is far from the bandgaps of Ge, we found that the most reasonable explanation is the onset of $L \to \Gamma$ intervalley scattering absorption (IVSA). IVSA has previously been observed in n-type Si [20], GaAs [21], and GaP [22], though not reported in n-type bulk Ge [12–15]. The 0.25% tensile strain in the n^+ Ge films enhances IVSA by decreasing the energy difference between L and Γ valleys and making more initial and final states accessible to phonon-assisted IVSA [16]. To confirm this interpretation, the absorption in Region II is subtracted by the intra-L-valley absorption to obtain IVSA absorption edges (dashed orange curve in Fig. 2). As shown in Fig. 3, IVSA edge shows a redshift with increasing n-type doping level. This IVSA edge approximately corresponds to the energy difference (ΔE) between the highest filled states in the L valleys (~Fermi level E_f) and the bottom of Γ valley, as illustrated in the inset of Fig. 3. The increase in n-type doping concentration raises the Fermi level and reduces ΔE, thereby leading to a redshift of the IVSA edge. The calculated ΔE using the method described in [3] is in good agreement with the experimental IVSA edge data, confirming the IVSA mechanism in Regime II. The strong intervalley scattering from L to Γ valleys promotes electronic occupation of the direct Γ valley, which in turn enhances direct gap light emission from Ge. Note that this IVSA-enhanced direct gap emission from Ge is exactly *opposite* to the case of III–V semiconductors, where IVSA from the direct Γ to indirect L valleys is the dominant source of optical loss at lasing wavelengths [16]. Together with the low intravalley FCA in the wavelength range of 1.5–1.7 μm, these two factors reduce the n-type doping level and injected carrier density required for electrically pumped Ge lasers.
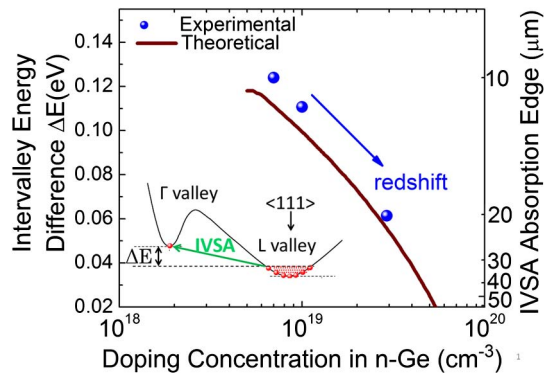
Fig. 3.   (Color online) Theoretical and experimental intervalley energy difference between L and Γ valleys as a function of doping concentration. The inset schematically illustrates the phenomenon of $L \rightarrow \Gamma$ IVSA in n^+ Ge.

Regime III in Fig. 2 shows a combined contribution of IVSA and indirect gap absorption. The steep absorption edge at ~1650 nm corresponds to the onset of direct gap absorption. We also found that, with the increase of n-type doping level, the boundary between direct and indirect transition becomes more and more blurry, which may be attributed to enhanced $L \rightarrow \Gamma$ intervalley scattering.

In conclusion, we report a strong $L \rightarrow \Gamma$ IVSA at $\lambda <$ 10 μm and a weak intra-L-valley free-electron absorption at the lasing wavelength regime of $\lambda = 1.5$–1.7 μm from tensile-strained n^+ Ge-on-Si gain media. The strong $L \rightarrow \Gamma$ intervalley scattering favors electronic occupation of the direct Γ valley to enhance the direct gap optical gain, while the low intravalley free-electron absorption leads to low optical losses. These two factors lead to a higher net gain in electrically pumped Ge-on-Si lasers than anticipated, indicating that a Ge-on-Si laser can potentially achieve a much better performance than our original theoretical prediction in [3].

References

1. D. H. Ahn, C. Y. Hong, J. F. Liu, M. Beals, W. Giziewicz, L. C. Kimerling, and J. Michel, Opt. Express **15**, 3916 (2007).
2. J. F. Liu, M. Beals, A. Pomerene, S. Bernardis, R. Sun, J. Cheng, L. C. Kimerling, and J. Michel, Nat. Photonics **2**, 433 (2008).
3. J. Liu, X. Sun, D. Pan, X. X. Wang, L. C. Kimerling, T. L. Koch, and J. Michel, Opt. Express **15**, 11272 (2007).
4. J. F. Liu, L. C. Kimerling, and J. Michel, Semicond. Sci. Technol. **27**, 094006 (2012).
5. J. F. Liu, X. Sun, R. Camacho-Aguilera, L. C. Kimerling, and J. Michel, Opt. Lett. **35**, 679 (2010).
6. R. E. Camacho-Aguilera, Y. Cai, N. Patel, J. T. Bessette, M. Romagnoli, L. Kimerling, and J. Michel, Opt. Express **20**, 11316 (2012).
7. J. F. Liu, X. Sun, L. C. Kimerling, and J. Michel, Opt. Lett. **34**, 1738 (2009).
8. B. Garrido, J. A. Moreno, J. Samitier, and J. R. Morante, Appl. Surf. Sci. **63**, 236 (1993).
9. M. K. Gunde and B. Aleksandrov, Appl. Opt. **30**, 3186 (1991).
10. W. Kaiser, P. H. Keck, and C. F. Lange, Phys. Rev. **101**, 1264 (1956).
11. A. R. Bean, R. C. Newman, and R. S. Smith, J. Phys. Chem. Solids **31**, 739 (1970).
12. H. Y. Fan, W. Spitzer, and R. J. Collin, Phys. Rev. **101**, 566 (1956).
13. R. Rosenberg and M. Lax, Phys. Rev. **112**, 843 (1958).
14. W. G. Spitzer, F. A. Trumbore, and R. A. Logan, J. Appl. Phys. **32**, 1822 (1961).
15. C. Haas, Phys. Rev. **125**, 1965 (1962).
16. C.-Y. Tsai, C.-H. Chen, T. L. Sung, T.-Y. Wu, and F.-P. Shih, IEEE. J. Quantum Electron. **34**, 552 (1998).
17. O. Madelung, ed., *Physics of Group IV Elements and III–V Compounds*, Vol. **17a** of Landolt–Börnstein: Numerical Data and Functional Relationships in Science and Technology (Springer, 1982).
18. Y. Cai, Z. Han, X. Wang, R. Camacho-Aguilera, L. C. Kimerling, J. Michel, and J. Liu, "Analysis of threshold current behavior of bulk and quantum well germanium laser structures," IEEE J. Sel. Top. Quantum Electron., doc. ID JSTQE-INV-SL-04810-2012.R1 (to be published).
19. A. Haug, Semicond. Sci. Technol. **7**, 373 (1992).
20. W. Spitzer and H. Y. Fan, Phys. Rev. **108**, 268 (1957).
21. W. G. Spitzer and J. M. Whelan, Phys. Rev. **114**, 59 (1959).
22. J. D. Wiley and M. Didqmenico, Phys. Rev. B **1**, 1655 (1970).